# Auger electron emission following double electron capture in 150-keV $Ne^{10+}$ + He collisions

F. Fremont, H. Merabet, J. Y. Chesnel, X. Husson, A. Lepoutre, D. Lecler, and G. Rieger
*Laboratoire de Spectroscopie Atomique, Institut des Sciences de la Matière et du Rayonnement, Boulevard du Maréchal Juin, 14000 Caen, France*

N. Stolterfoht
*Hahn-Meitner Institut, Bereich Festkörperphysik, Glienickerstrasse 100, D-14109 Berlin, Germany*
(Received 29 April 1994)

The method of projectile electron spectroscopy was used to measure the $Ne^{8+}$ Auger decay of the configurations $3lnl'$ and $4lnl'$ ($n \geq 4$) created by double electron capture in 150-keV $Ne^{10+}$ + He collisions. Auger yields were evaluated to convert the experimental cross sections for Auger-electron emission into the corresponding cross sections for double electron capture. It is found that the cross sections attributed to the configurations $3lnl'$ follow a $n^{-3}$ law, while the excitation of the configurations $4lnl'$ is rather selective for $n = 5$. It is shown by means of model calculations that the electron correlation plays a decisive role in the capture mechanisms producing the configurations $3lnl'$.

PACS number(s): 32.80.Hd, 34.50.Fa

## INTRODUCTION

During the last few years, double electron capture into slow, highly charged ions interacting with gas atoms has received much attention. Processes for double capture have been studied extensively by means of translational energy spectroscopy [1,2], photon spectroscopy [3,4], and Auger-electron spectroscopy [5,6]. Double capture leads to doubly excited states and current interest concerns the production mechanisms of these states.

The mechanisms responsible for double electron capture are illustrated in Fig. 1, which shows the orbital electron energies for the $(Ne+He)^{10+}$ system. In the incident channel, two electrons occupy the He $1s$ orbital that crosses the $4l$ and $5l$ orbitals of neon near 5 and 9 a.u., respectively. In this region, the uncorrelated double electron capture may occur by two independent one-electron transitions, creating the configurations of near equivalent electrons $4l5l'$. As the internuclear distance continues to decrease, resonance conditions are created for the correlated-double-capture (CDC) process, in which one electron is transferred into the $3l$ orbital while another one is excited into a Rydberg level $nl$. Alternatively, the $3l$ and $nl$ orbitals may be populated by one-electron capture into the $4l$ orbital followed by a correlated transfer and excitation (CTE) process.

In this work, we measure double capture cross sections in 150-keV $Ne^{10+}$ + He collisions. The study of this system is of considerable interest because it gives specific information on the mechanisms responsible for double capture at low energy. The double capture mechanisms are more complex than those for $C^6$+He [7], previously studied in detail. Nevertheless, both systems exhibit similarities. The configurations of equivalent and nonequivalent electrons $3lnl'$ and $4lnl'$ ($n \geq 4$) can be studied. They correspond to the $2lnl'$ and $3lnl'$ configurations in the collision system $C^{6+}$ + He, respectively. The $3lnl'$ ($4lnl'$) configurations are partially autoionizing, giving rise to $L$-shell ($M$-shell) Auger electrons whose energies are in the range 80–190 eV. These electrons can be studied by means of high-resolution Auger spectroscopy.

We also calculated x-ray and Auger transition rates for these configurations by means of the Hartree-Fock atomic structure code by Cowan [8], which indicates that the Auger yield is rather constant for the configurations $3lnl'$ ($n = 4$–10). Using the theoretical Auger yields, we determined cross sections for the production of the configurations $3lnl'$ and $4lnl'$ ($n \geq 4$). The production of these configurations will be discussed from the perspective of electron-correlation effects during the collision.

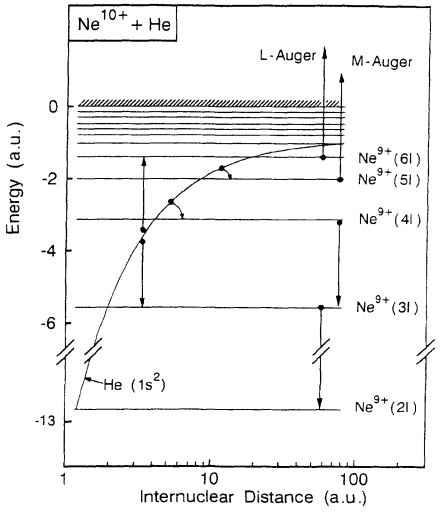


FIG. 1. Diagram of orbital electron energies for the system $(Ne+He)^{10+}$ showing correlated and uncorrelated double electron capture. These processes produce configurations that decay by $L$-Auger and $M$-Auger electron emission, respectively.

 

## EXPERIMENTAL METHOD AND DATA ACQUISITION

The experimental setup and the method to evaluate cross sections have been developed previously [6,7,9], so only a few details are given below. The experiments were performed at the test bench of the 14-GHz ECR ion source at the Grand Accelerateur National d'Ions Lourds (GANIL) in Caen. The electron-spectroscopy apparatus [9] from the Hahn-Meitner Institut (HMI) in Berlin was utilized. The $Ne^{10+}$ ions, extracted at an energy of 15 keV, were magnetically analyzed and focused to a diameter of about 2 mm. Typical beam currents of about 15 nA were collected in a Faraday cup and were used to normalize the spectra. In the scattering chamber, a base pressure of some $10^{-7}$ Torr was achieved. In the center of the chamber a gas jet was installed providing an atomic beam target. The jet consists of a simple tube with an inner diameter of 1 mm. During the acquisition, a pressure of $\sim 5\times 10^{-6}$ Torr was maintained in the chamber. This pressure was sufficiently low to avoid, in principle, multiple-charge-exchange collisions for the incident $Ne^{10+}$ ions.

Auger electrons produced after the collision were detected at several angles up to 140°, with respect to the incident-beam direction, using a tandem electron spectrometer [9] that consists of two consecutive 90° parallel-plate analyzers. The entrance analyzer deflects the electrons out of the ion beam and suppresses background electrons. The intrinsic resolution of the exit analyzer was 5% full width at half maximum (FWHM). A constant energy resolution of 1 eV was achieved by deceleration of the electrons in the region between the analyzers to 20 eV. The electron acceptance angle was $\Delta\theta\approx 2°$. The length $l_o$ of the ion beam, as seen by the spectrometer at 90° with respect to the incident beam, was 4.4 mm. This length increases according to $l_f = l_o/\sin\theta$ as the observation angle decreases. Hence, a varying size of the gas jet beam is included in the observation window of the spectrometer.

To evaluate absolute cross sections, we have used a method previously described in detail [9]. Absolute values for the production of Auger electrons were obtained using a uniform-gas pressure in the scattering region. This was achieved by moving the jet upwards far away from the ion beam and flooding the scattering chamber uniformly with the He target gas. The uniform-target-gas mode was also used to determine the angular distribution of the Auger electrons. At several angles, Auger spectra were measured with low resolution (i.e., high efficiency) both with the gas jet and in the uniform-gas mode. The results were used to normalize the angular distributions obtained with high resolution.

## DATA EVALUATION OF CROSS SECTIONS

Figure 2 shows typical $L$-shell Auger spectra at different observation angles. The most prominent lines are attributed to the configurations $3lnl'$, which are well separated for $n=4$ to 9. The line group centered at 180 eV can be attributed to the limit of the $3lnl'$ series and to the configurations $4l4l'$, decaying to the $2l\varepsilon l'$ configurations by means of Auger transitions. Since the Auger electrons originate from moving emitters, they are influenced by kinematic effects [10]. However, contrary to the $2lnl'$ configurations produced in the collision system $C^{6+}+He$ [7], the spectra are not strongly affected by line-broadening effects. This is due to the fact that the $3lnl'$ lines from $Ne^{10+}+He$ are lower in energy than the corresponding $2lnl'$ lines from the $C^{6+}+He$ system. Using the formulas given previously [10], total linewidths of about 0.6, 0.82, and 0.97 eV were estimated for the observations angles of 0°, 20°, and 75°, respectively.

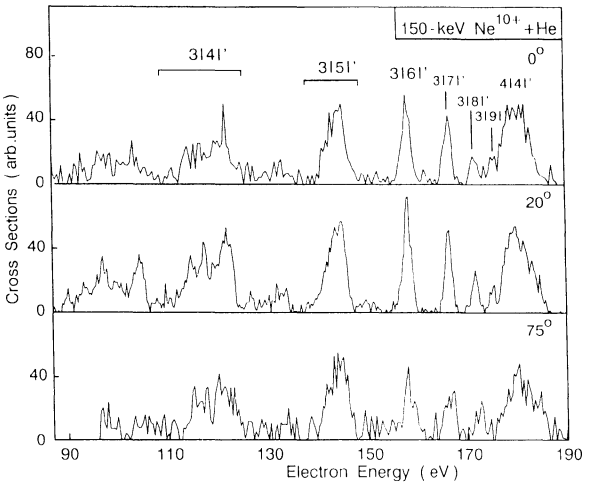


FIG. 2. High-resolution spectra of $L$-shell Auger electrons produced in 150-keV $Ne^{10+}+He$ collisions at a few angles. Each peak corresponds to the decay of states associated with a configuration $3lnl'$ ($n=4$–9). The peak centered at 200 eV corresponds to the limit of the $3lnl'$ series and to the configurations $4l4l'$, which decay to $2l\varepsilon l'$ configurations. Double collisions give rise to $1s3lnl'$ configurations representing ~25% of the total intensity.

Due to the low pressure in the scattering chamber, we expect to be in a single-collision mode. Nevertheless, in addition to the $3lnl'$ configurations, we observe lines due to Li-like configurations ($1s3lnl'$) that can only be produced by multiple collisions. The intensity of the Li-like peaks represents 25% of the total intensity. This value is larger than that obtained by a simple calculation, which shows that the intensity should not be more than 15%. We may expect that charge changing collisions also occur at the slit edges.

Our attention is now focused on groups of states formed by the configurations $3lnl'$ and $4lnl'$. The measured Auger spectra were used to evaluate single-differential cross sections $d\sigma^n_{3lnl'}/d\Omega$ for Auger electron emission attributed to a given configuration $3lnl'$. Thus the corresponding electron spectra obtained with high resolution were numerically integrated with respect to the electron energy. The results are given in Table I and Fig. 3. The absolute uncertainties are 30% and the relative uncertainties, with respect to a variation of the emission angle, are 20%. The relative uncertainties increase to 30% for the configurations $3l9l'$. The single-differential cross sections are found to be isotropic within

TABLE I. Single-differential Auger emission cross sections $d\sigma^a_{nln'l'}/d\Omega$ for the configurations $3lnl'$ ($n \geq 4$). The data are obtained by integration of the spectra partially given in Figs. 2 and 3. The observation angle refers to the laboratory rest frame.

| Angle | Cross section $d\sigma^a_{nln'l'}/d\Omega$ ($10^{-18}$ cm$^2$/sr) | | | | | |
|---|---|---|---|---|---|---|
| (deg) | $3l4l'$ | $3l5l'$ | $3l6l'$ | $3l7l'$ | $3l8l'$ | $3l9l'$ |
| 0 | 3.45 | 2.92 | 1.37 | 0.86 | 0.45 | 0.28 |
| 20 | 3.73 | 2.39 | 1.34 | 0.82 | 0.38 | 0.23 |
| 40 | 3.10 | 2.40 | 1.30 | 0.80 | 0.34 | |
| 60 | 2.90 | 2.30 | 1.00 | 0.80 | 0.45 | |
| 75 | 3.27 | 2.45 | 1.10 | 0.80 | 0.44 | |
| 90 | 3.57 | 2.60 | 1.25 | 0.80 | 0.37 | |
| 120 | 3.15 | 1.98 | 0.98 | 0.80 | 0.34 | |
| 140 | 2.77 | 2.01 | 1.24 | 0.80 | 0.40 | |

the experimental uncertainties for the configurations $3lnl'$ ($n \geq 5$). For the configurations $3l4l'$, the cross sections are anisotropic with a maximum at 0° and 180°.

Figure 4 shows an example of the measured $M$-Auger spectrum, acquired with high resolution at the observation angle of 20°. It indicates the peak structure associated with the configurations $4lnl'$ ($n = 5,6$). Assuming an isotropic distribution of the Auger electrons, the cross sections $d\sigma^a_{4lnl'}/d\Omega$ were multiplied by $4\pi$ to evaluate total cross sections for Auger-electron emission (Table II).

The results for the cross sections are given in Table II, including the configurations $3lnl'$ and $4lnl'$. It is found that Auger-electron emission cross sections for the $3lnl'$ configurations follow a $n^{-3}$ law. This finding agrees with the cross-section data obtained for configurations $2lnl'$ in the collision system 90-keV $C^{6+}$ + He [7,11].

The average $L$- and $M$-Auger yields $a_L(n)$ and $a_M(n)$ for the configurations $3lnl'$ ($n = 4$–$8$) and $4lnl'$ ($n = 4,5$),

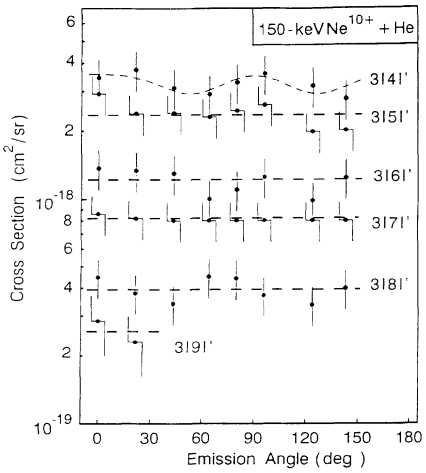


FIG. 3. Single-differential cross sections for the emission of Auger electrons associated with the configurations $3lnl'$ ($n = 4$–$9$). The data are obtained by integration of the spectra partially given in Fig. 3. The observation angle refers to the projectile rest frame. The dashed curves represent a fit to the experimental data.

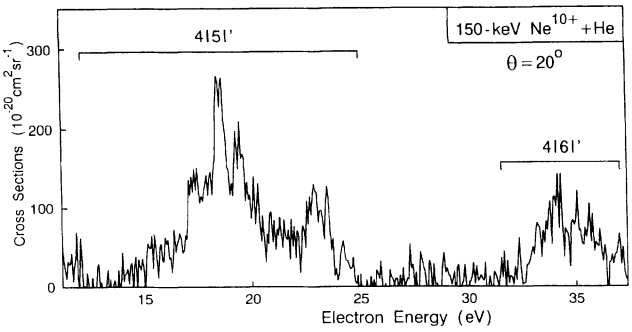


FIG. 4. High-resolution spectra of $M$-shell Auger electrons produced in 150-keV $Ne^{10+}$ + He collisions at the observation angle of 20°. The peaks correspond to the decay of states associated with the configurations $4lnl'$ ($n = 5$–$6$).

respectively, were calculated by means of the Hartree-Fock code of Cowan [8] (cf. Table II). Similar calculations have been done previously [12]. Transitions rates for radiative and nonradiative decay for the states $|3lnl'\,^{2S+1}L_J\rangle$ and $|4lnl'\,^{2S+1}L_J\rangle$ were evaluated to determine the associated individual $L$- and $M$-Auger yields $a_L(3lnl'\,^{2S+1}L_J)$ and $a_M(4lnl'\,^{2S+1}L_J)$. The average Auger yields for a given $n$ were obtained by means of the expression

$$a_{L,M}(n') = \sum_{l,l'S,J} Q_{n'}(l,l',J)\, a_{L,M}(nln'l'\,^{2S+1}L_J) , \quad (1)$$

where $Q_{n'}(l,l',J)$, with the normalization $\sum_{l,l',J} Q_{n'}(l,l',J) = 1$, is the probability for the production of the state $|nln'l'\,^{2S+1}L_J\rangle$ for given $n$ and $n'$. A simple model, in which this probability is factorized [7], was used,

TABLE II. Total Auger emission cross sections $\sigma^a_{nln'l'}$ for the configurations $3lnl'$ and $4lnl'$ ($n \geq 4$), obtained multiplying $d\sigma^a_{nln'l'}/d\Omega$ by $4\pi$. Under the assumption that the Auger emission cross sections for the configurations $3lnl'$ follow an $n^{-3}$ law, the Auger emission cross sections for the configurations $4l4l'$ were measured by subtraction of the integration with the cross sections for the configurations $3lnl'$ ($n \geq 10$). Also given are the corresponding Auger yields $a_l(n)$. The total production cross sections $\sigma_{nln'l'}$ are obtained by dividing $\sigma^a_{nln'l'}$ by the related Auger yield. The indicated errors account only for uncertainties due to statistics and background subtraction.

| Configuration | $\sigma^a_{nln'l'}$ ($10^{-17}$ cm$^2$/sr) | $a_l(n)$ | $\sigma_{nln'l'}$ ($10^{-16}$ cm$^2$) |
|---|---|---|---|
| $3l4l'$ | 4.07±1.22 | 0.82 | 0.52±0.16 |
| $3l5l'$ | 2.99±0.90 | 0.76 | 0.39±0.12 |
| $3l6l'$ | 1.50±0.45 | 0.68 | 0.23±0.07 |
| $3l7l'$ | 1.02±0.31 | 0.64 | 0.16±0.05 |
| $3l8l'$ | 0.50±0.15 | 0.59 | 0.093±0.03 |
| $3l9l'$ | 0.33±0.13 | 0.58 | 0.060±0.02 |
| $4l4l'$ | 6.28±1.88 | 0.80 | 0.79±0.24 |
| $4l5l'$ | 9.80±2.94 | 0.89 | 1.10±0.33 |
| $4l6l'$ | 2.35±0.71 | 0.79 | 0.30±0.09 |
| $4l7l'$ | 0.88±0.26 | 0.80 | 0.11±0.03 |

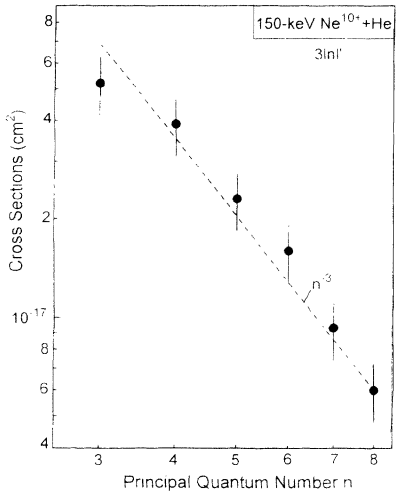


FIG. 5. Cross sections for the production of the configurations $3lnl'$ ($n=4$–9) in 150-keV $Ne^{10+}+He$ collisions. The dashed line, representing the $n^{-3}$ law, is normalized to fit the experimental data.

$$Q_{n'}(l,l',J)=q_n(l)q_{n'}(l')p(J)\ , \tag{2}$$

where $q_n(l)$, $q_{n'}(l')$, and $p(J)$ are the occupation probabilities associated with the quantum numbers $l$, $l'$, and $J$, respectively. The probability $p(J)$ is set to be proportional to $2J+1$. The probabilities $q_n(l)$ and $q_{n'}(l')$ were estimated using the model by Burgdörfer, Morgenstern, and Niehaus [13]. More details of the Auger yield analysis will be given elsewhere [14].

Results of the average Auger yields are given in Table II. It is seen that the average Auger yields for the configurations $3lnl'$ decrease slowly with $n$. The average Auger yields for the configurations $4lnl'$ ($n=4$–7) are close to unity.

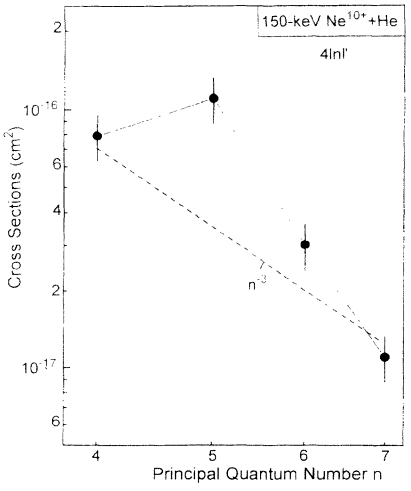


FIG. 6. Cross sections for the production of the configurations $4lnl'$ ($n=4$–7) in 150-keV $Ne^{10+}+He$ collisions. The dashed line, representing the $n^{-3}$ law, is drawn to show the selectivity of the cross sections.

The calculated average $L$- and $M$-Auger yields were used to determine the cross sections $\sigma_{nln'l'}$ for the production of the configurations $3lnl'$ ($n=4$–9) and $4lnl'$ ($n=4$–7). The results (Table II and Figs. 5 and 6) are obtained dividing Auger emission cross sections by the related average Auger yield. It is recalled that Auger emission cross sections for the production of the $3lnl'$ configurations follow the $n^{-3}$ law. Since the Auger yield is rather constant, the double capture cross section for producing the configurations $3lnl'$ also follow the $n^{-3}$ law. It was noted [6,7,11] that the $n^{-3}$ law may be a signature for the dielectronic processes, as discussed in the following section.

## DISCUSSION

The different processes for the production of the $3lnl'$ and $4lnl'$ ($n\geq 4$) configurations by $Ne^{10+}$ impact are discussed by means of the potential curves given in Figs. 7 and 8, respectively. The final energies are determined by Coulombic potentials $Q/R-E$, where $Q=9$ and 16 for single and double capture, respectively, $R$ is the internuclear distance, and $E$ is the asymptotic binding energy of the electrons involved during the collision.

The incident channel $Ne^{10+}+He$ crosses two potential curves labeled asymptotically $Ne^{9+}(4l)+He^{+}$ and $Ne^{9+}(5l)+He^{+}$ near 5 and 9 a.u., respectively, where a single-electron transition may occur due to the nucleon-electron interaction (Fig. 7). Cross sections for these monoelectronic transitions are calculated using the Landau-Zener model [15]. The transition probability is obtained as

$$p(b)=1-\exp\left[-\frac{2\pi|H_{if}^{C}|^2}{v_R F(R_C)}\right]\ , \tag{3}$$

where $b$ is the impact parameter, $N_f$ is the number of

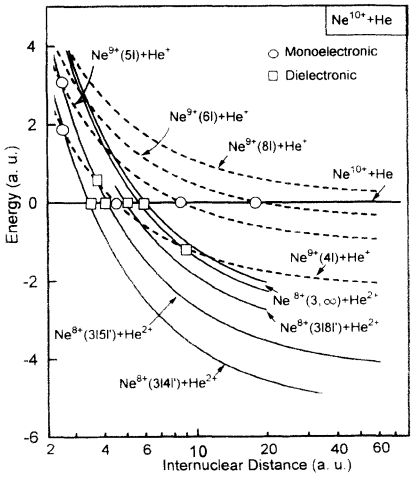


FIG. 7. Potential-curve diagram for the system $Ne^{10+}$ + He. The diagram shows potential curves relevant for the production of configurations $3lnl'$ ($n=4$–7). Dashed lines and solid lines correspond to single and double capture, respectively. Transitions at crossings identified by a circle are caused by a one-electron interaction, whereas transitions at crossings identified by a square are caused by a two-electron interaction.

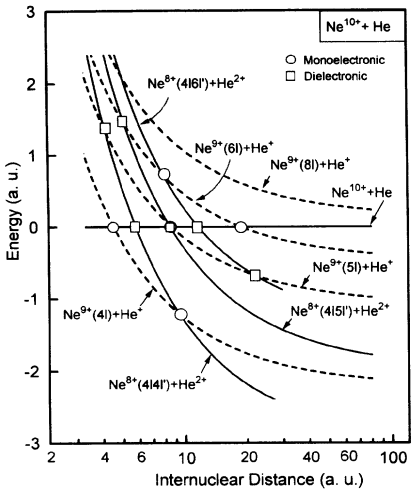


FIG. 8. Potential-curve diagram for the system $Ne^{10+}+He$. The diagram shows potential curves relevant for the production of configurations $4lnl'$ ($n=4$–7). Dashed lines and solid lines correspond to single and double capture, respectively.

final states, $v_R$ is the radial velocity, and $F(R_C)$ is a measure of the relative inclination of the potential curves at the crossing radius $R_C$. The matrix element $H_{if}$ was calculated using the method by Olson and Salop [16]. The calculations by the Landau-Zener model show that the single-electron transfer populates preferentially the $5l$ state (Table III).

At about 3 a.u., a further monoelectronic transition may produce the $3l4l'$ and $3l5l'$ configurations. Thus, two uncorrelated single-electron transitions are likely to create the configurations of quasiequivalent electrons. Furthermore, the $3l4l'$ and $3l5l'$ configurations may be populated directly at internuclear distances of about 3.5 and 4.5 a.u., respectively, by means of a correlated-double-capture process (CDC). The crossings are identified in the figure by squares. It is also seen in Fig. 7 that the correlated transfer and excitation may produce, *via* a first capture into the level $4l$, the configurations $3l5l'$. Both processes, in which the electron-electron interaction is dominant, are examples for the dielectronic process of *autoexcitation* [17].

TABLE III. Single capture cross sections $\sigma_n$ for producing the configurations $nl$ estimated with the Landau-Zener model for the system 150-keV $Ne^{10+}+He$. The matrix element $H_{12}$ was evaluated using the formula by Olson and Salop [16]. The configuration $5l$ is preferentially populated. The quantity $R_C$ is the crossing radius.

| State | $R_C$ (a.u.) | $H_{12}$ (a.u.) | $\sigma_n$ ($10^{-16}$ cm$^2$) |
|---|---|---|---|
| $3l$ | 1.9 | 0.97 | 0.52 |
| $4l$ | 4.1 | 0.29 | 17.2 |
| $5l$ | 8.2 | 0.028 | 38.0 |
| $6l$ | 18.5 | $8.5\times10^{-5}$ | 0.014 |

The incident channel also crosses the state labeled $Ne^{8+}(3l8l')+He^{2+}$ around 5 a.u., where the CDC process may produce configurations of nonequivalent electrons. From the diagram in Fig. 7, it is seen that the configurations $3lnl'$ ($n\geq8$) are not likely to be produced by two successive monoelectronic transitions. This is due to the fact that no crossing appears between the incident channel and the $Ne^{9+}(nl,\ n\geq8)+He^{+}$ channel. Alternatively, these configurations may be populated by a CTE process following the monoelectronic transfer into the $Ne^{9+}(5l)$ or $Ne^{9+}(4l)$ states.

The mechanisms for the production of the configurations $4lnl'$ ($n\geq4$) (Fig. 8) are similar to those for the production of the configurations $3lnl'$. However, there exist characteristic differences between the two cases. The configurations $4l6l'$ may be populated by means of independent monoelectronic transitions or a CDC process. It is seen from Fig. 6 that the crossings between the entrance channel and the exit channels $Ne^{9+}(5l)+He^{+}$ and $Ne^{8+}(4l5l')+He^{2+}$ occur at about the same internuclear distance. Hence, in this case, it is difficult to distinguish between monoelectronic and dielectronic processes.

We consider now the configurations $4l4l'$, which may be populated by two single transitions involving a capture into the $4l$ configurations (Fig. 8). We also see from Fig. 8 that a dielectronic CDC process may occur at about 6 a.u. In addition to these processes, a further dielectronic mechanism (CTE process) may produce the configurations $4l4l'$. Near 8 a.u., a single-electron transition may take place (Fig. 8), followed, at about 4 a.u., by a dielectronic process denoted inverse autoexcitation [18]. The $5l$ electron is dropped to the $4l$ level and, by electron-electron interaction, it gives its energy to the second electron, which is transferred into the $4l$ level.

Using the Landau-Zener formula (1), we evaluated the cross sections for the production of the configurations $3lnl'$ and $4lnl'$ by two monoelectronic transitions (Table IV). The dominant capture occurs on the configurations $3l4l'$, $3l5l'$, and $4l5l'$. It is found that the cross sections for the production of the configurations $4l4l'$, $3lnl'$, and $4lnl'$ ($n\geq6$) are rather small. Hence, if these configurations are created, we must invoke other mechanisms such as dielectronic processes produced by the electron-electron interaction.

It has been previously shown in detail [6,7,19] that dielectronic processes are responsible for the production of the configurations $2lnl'$ of nonequivalent electrons in the system $C^{6+}+He$. Similarly, for the system $Ne^{10+}+He$, we would expect that electronic correlation dominates the nonequivalent electron configurations $3lnl'$. In the following, it is shown by means of Landau-Zener estimates that dielectronic processes are likely to be dominant for the production of the configurations $3lnl'$ ($n\geq6$). For small perturbations, it follows from Eq. (3) that

$$p(b)=N_f\frac{2\pi|H_{if}^{C}|^2}{v_R F(R_C)}\ , \tag{4}$$

where the notation of Eq. (3) is used. The quantity $H_{if}^{C}$ is

TABLE IV. Double capture cross sections $\sigma_{nln'l'}$ for production of the configurations $3lnl'$ and $4lnl'$ estimated by means of a two-step Landau-Zener model for the system 150-keV $Ne^{10+}+He$. The crossing radii $R_{12}$ and $R_{23}$ correspond to the first and second capture, respectively. The matrix elements $H_{12}$ and $H_{23}$ were evaluated using the formulas of Olson and Salop [16] and Chibisov and Janev [20], respectively. It is seen that two monoelectronic transitions cannot populate the configurations $4l4l'$ and $3lnl'$ ($n \geq 6$). Hence we expect a dielectronic process to explain the creation of these configurations during the collision.

| Configuration | $R_{12}$ (a.u.) | $R_{23}$ (a.u.) | $H_{12}$ (a.u.) | $H_{23}$ (a.u.) | $\sigma_{nln'l'}$ $10^{-16}$ cm$^2$ |
|---|---|---|---|---|---|
| $3l4l'$ | 4.05 | 2.34 | 0.29 | 0.33 | 8.7 |
| $3l5l'$ | 8.21 | 2.15 | 0.03 | 0.37 | 1.5 |
| $3l6l'$ | 18.5 | 2.06 | $8\times10^{-5}$ | 0.38 | $8\times10^{-4}$ |
| $4l4l'$ | 4.05 | 8.86 | 0.29 | $10^{-3}$ | $3.6\times10^{-2}$ |
| $4l5l'$ | 8.21 | 7.95 | 0.03 | $2.7\times10^{-3}$ | 0.27 |
| $4l6l'$ | 18.5 | 7.52 | $8\times10^{-5}$ | $4\times10^{-3}$ | $2.5\times10^{-3}$ |

the dielectronic matrix element associated with the operator $H^C$, which is responsible for the dielectronic transition.

The dielectronic matrix element $H_{if}^C$ is given by

$$H_{if}^C=\left\langle \varphi_f^1\varphi_f^2 \left| \frac{1}{|\mathbf{r}_1-\mathbf{r}_2|} \right| \varphi_i^1\varphi_i^2 \right\rangle , \tag{5}$$

where $\varphi_i^k$ and $\varphi_f^k$ are, respectively, the initial and final orbitals of the electron labeled $k=1$ or 2. The asymptotic matrix element $H_{if}^C$ can be written as [20,21]

$$H_{if}^C=ke^{-\alpha R_C}Zn^{-3/2} , \tag{6}$$

where $k$ is approximately constant for a given system and $\alpha\approx0.43(\sqrt{2I_A}+\sqrt{2I_B})$. The quantities $I_A$ and $I_B$ are the binding energies of the electrons involved in the charge transfer between the collision partners $A$ and $B$. The factor $Zn^{-3/2}$ (where $Z$ is the atomic number of the projectile and $n$ is the principal quantum number of the outer electron captured by the projectile) is the level density following from the Rydberg formula. It is noted that this factor creates the $n^{-3}$ dependence of the cross sections for large values of $n$.

To evaluate the probability for a direct transition to a configuration $3lnl'$, it is necessary to determine the dielectronic matrix element $H_{if}^C$. Hence the value of $k$ is needed. According to Chibisov and Janev [20], $k$ depends on the crossing radius $R_C$ and on the atomic number of the projectile $Z$. From the comparison of the experimental data for the present system, it follows that the quantity $k$ for the system $Ne^{10+}+He$ is of the same order of magnitude as that for $C^{6+}+He$. For the latter system, this constant was evaluated to be $k=0.3$ [21].

For $Ne^{10+}+He$, cross sections for the production of the configurations $3lnl'$ ($n=4-9$) were calculated with $k\approx0.5$, and the comparison was made with our experimental data (Table V). For $n=4$ and 5, it is noted that our calculations deviate noticeably from experimental data by a factor of about 10. Hence, it appears that alternative mechanisms, such as the monoelectronic processes estimated in Table IV, are responsible for the production of the configurations $3l4l'$ and $3l5l'$. However, it is seen for $n=6-9$ that our estimations agree fairly well with the experimental results. Hence, we conclude that dielectronic CDC and CTE processes are likely to be responsible for the production of the configurations $3ln'l'$ ($n \geq 6$).

Recently, the production of the $3lnl'$ configurations ($n \geq 10$) has been discussed by Bachau, Roncin, and Harel [22]. They explained the creation of these configurations in terms of a capture into $4l4l'$ configurations, followed by an electron-electron interaction between $4l4l'$ and $3lnl'$ configurations in the postcollision region. This postcollision interaction only affects the configurations $3lnl'$ ($n \geq 10$), i.e., with $n$ higher than those for the dominant lines measured in this work. In view of the present study, it would be useful to also study the creation of the configurations $3lnl'$ ($n \geq 10$), which are created by dielectronic processes during the collision and not in the postcollision region. We propose more experimental and theoretical work to verify the two types of processes.

Finally, we consider the production of the configurations $4lnl'$. Figure 6 shows that the Auger-electron emission is rather selective. Dividing the Auger-electron emission cross sections $\sigma_{nln'l'}^a$ by the average Auger yield, which is constant for $n=4-7$, the selectivity remains. The double capture on the configuration $4l5l'$ is dominant. The corresponding cross sections for $n=5-7$ are roughly proportional to $n^{-7}$. The same

TABLE V. Double capture cross sections for the production of the configurations $3lnl'$ in the system 150-keV $Ne^{10+}+He$ calculated by means of the Landau-Zener model. The dielectronic matrix element $H_{if}^C$ has been evaluated an asymptotic formula [20,21]. In the last column, experimental Auger emission cross sections are given (cf. Table II).

| $Ne^{10+}+He$ Configuration | $H_{if}^C$ (a.u.) | $\sigma_{3lnl'}$ ($10^{-17}$ cm$^2$) | $\sigma_{3lnl}^{expt}$ ($10^{-17}$ cm$^2$) |
|---|---|---|---|
| $3l4l'$ | $1.4\times10^{-3}$ | 0.5 | 5.2±1.6 |
| $3l5l'$ | $9.4\times10^{-4}$ | 0.8 | 3.9±1.1 |
| $3l6l'$ | $8.2\times10^{-4}$ | 3.2 | 2.3±0.7 |
| $3l7l'$ | $3.7\times10^{-4}$ | 1.2 | 1.6±0.5 |
| $3l8l'$ | $2.0\times10^{-4}$ | 0.64 | 0.93±0.30 |
| $3l9l'$ | $1.2\times10^{-4}$ | 0.36 | 0.60±0.20 |

behavior in single-electron capture has been observed in the collision $O^{6+}(1s2s)+He$ [23]. In this case, one may conclude in accordance with single-electron capture that electron-nucleon interaction plays the dominant role for the configurations $4lnl'$ during the collision.

## CONCLUSION

We studied the emission of Auger electrons originating from the decay of states associated with configurations $3lnl'$ ($n=4-9$) and $4lnl'$ ($n=4-7$) of nonequivalent and quasiequivalent electrons. The angular distributions of the $3lnl'$ electrons were found to be isotropic, except for $3l4l'$. The differential Auger-electron emission cross sections were integrated assuming an isotropic distribution of Auger electrons. Average Auger yields for the configurations $3lnl'$ and $4lnl'$ were derived by means of Hartree-Fock calculations. The calculated Auger yields decrease slowly with $n$ for the configurations $3lnl'$, and are constant, i.e., close to unity, for the configurations $4lnl'$. With the knowledge of the Auger yield, it was possible to determine the $3lnl'$ and $4lnl'$ production cross sections. It is found that cross sections for producing the configurations $3lnl'$ follow approximately the well known $n^{-3}$ law, while the production of the configurations $4lnl'$ is rather selective. We conclude that two different processes are responsible for the production of the configurations $3lnl'$ and $4lnl'$.

The discussion of the capture mechanisms is based on schematic diagrams of approximate potential curves, previous experimental data, and model calculations. It is seen from potential-curve diagrams that configurations of equivalent or quasiequivalent electrons may be populated by uncorrelated single-electron transitions. The strong selectivity of the capture into the configurations $4l5l'$ should be compared with the selectivity in the corresponding single-electron capture process. Such comparison was made for the single-electron capture in the collision $O^{6+}(1s2s)+He$ at low energy, in which the $3l$ level is dominantly populated. The single capture is governed by the Coulombic interaction between the target electron and the projectile nucleus. Hence, the configurations $4lnl'$ may be populated by electron-nucleus interaction. According to calculations and Fig. 7, the electron-nucleus interaction is likely to be responsible for the production of the configurations $3l4l'$ and $3l5l'$.

The mechanisms for the production of the configurations $3lnl'$ ($n\geq 6$) are discussed under the perspective of electron-correlation effects that occur during the collision. In analogy with the systems $C^{6+}+He$ and $O^{6+}+He$, for which many authors clearly show the importance of electron correlation, the processes produced by electron-correlation effects are used to understand the production of nonequivalent configurations. This conclusion is supported by the observed $n^{-3}$ dependence of the cross sections for the production of the configurations $3lnl'$ (see the configurations $2lnl'$ in the systems $C^{6+}+He$ and $O^{6+}+He$). Finally, cross sections for the production of the configurations $3lnl'$ have been determined on the basis of theoretical estimations [20,21], assuming uniquely dielectronic processes. The calculations provide evidence that dielectronic processes during the collision are responsible for the creation of the configurations $3lnl'$ ($n\geq 6$).


[1] K. Okuno, H. Tawara, T. Iwai, Y. Kaneto, M. Kimura, N. Kobayashi, A. Matsumoto, S. Ohtani, S. Tagaki, and S. Turubushi, Phys. Rev. A **28**, 127 (1983).

[2] L. R. Andersson, J. O. P. Pedersen, A. Barany, J. P. Bangsgaard, and P. Hvelplund, J. Phys. B **22**, 1603 (1989).

[3] S. Bliman, J. J. Bonnet, D. Hitz, T. Ludcec, M. Druetta, and M. Mayo, Nucl. Instrum. Methods Phys. Res. Sect. B **27**, 579 (1987).

[4] D. Vernhet, A. Chetioui, J. P. Rozet, C. Stephan, K. Wohrer, A. Touati, M. F. Politis, P. Bouisset, D. Hitz, and S. Dousson, J. Phys. B **22**, 1603 (1989).

[5] A. Bordenave-Montesquieu, P. Benoît-Cattin, A. Gleizes, S. Dousson, and D. Hitz, J. Phys. B **18**, L195 (1985).

[6] N. Stolterfoht, C. C. Havener, R. A. Phaneuf, J. K. Swenson, S. M. Shafroth, and F. W. Meyer, Phys. Rev. Lett. **57**, 74 (1986).

[7] N. Stolterfoht, K. Sommer, J. K. Swenson, C. C. Havener, and F. W. Meyer, Phys. Rev. A **42**, 5396 (1990).

[8] R. D. Cowan, *The Theory of Atomic Structure and Spectra* (University of California Press, Berkeley, 1981).

[9] N. Stolterfoht, Z. Phys. **248**, 81 (1971); **248**, 92 (1971); A. Itoh, T. Schneider, G. Schiwietz, Z. Roller, H. Platten, G. Nolte, D. Schneider, and N. Stolterfoht, J. Phys. B **16**, 3965 (1983).

[10] N Stolterfoht, Phys. Rep. **146**, 315 (1987).

[11] F. Frémont, K. Sommer, D. Lecler, S. Hicham, P. Boduch, X. Husson, and N. Stolterfoht, Phys. Rev. A **46**, 222 (1992).

[12] H. W. van der Hart and J. E. Hansen, J. Phys. B **26**, 3297 (1993).

[13] J. Burgdörfer, R. Morgenstern, and A. Niehaus, J. Phys. B **19**, L507 (1987).

[14] H. Merabet, G. Cremer, F. Frémont, and N. Stolterfoht (unpublished).

[15] L. D. Landau, Phys. Sovietunion **2**, 46 (1932) and C. Zener, Proc. R. Soc. London, Sect. A **137**, 696 (1932).

[16] R. E. Olson and A. Salop, Phys. Rev. A **14**, 579 (1976).

[17] N. Stolterfoht, Phys. Scr. **42**, 192 (1990).

[18] V. V. Afrosimov, Yu. S. Gordeev, A. N. Zinoviev, D. H. Rasulov, and A. P Shergin, in *Abstracts of Papers of the Ninth International Conference on the Physics of Electronic and Atomic Collisions, Seattle, 1975* edited by J. S. Risley and R. Geballe (University of Washington, Seattle, 1975), p. 1066.

[19] C. Harel, H. Jouin, and B. Pons, J. Phys. B **24**, L425 (1991).

[20] M. I. Chibisov and R. K. Janev, Phys. Rep. **166**, 1 (1988).

[21] N. Stolterfoht, Phys. Scr. T **46**, 22 (1993).

[22] H. Bachau, P. Roncin, and C. Harel, J. Phys. B **25**, L109 (1992).

[23] F. Frémont, H. Merabet, A. Lepoutre, D. Lecler, and N. Stolterfoht (unpublished).